Supplementary Material to

"Robust Control of Wireless Power Transfer Despite Load and Data Communications Uncertainties"

DOI:10.1109/JESTPE.2020.3033001,2020

Reza Naghash, Seyed Mohammad Mahdi Alavi, Seyed Ebrahim Afjei

***Abstract*—This is a supplementary material to [*S1*], which provides further information about fundamentals of the series-series compensation circuits in wireless power transfer (WPT) systems, and proportional-integral (PI) controllers designed by using the fixed-structure H_∞ [*S2*], and Skogestad internal model control (SIMC) [*S3*, *S4*] methods. It also provides complementary results, and discussions to [*S1*].**

S.I. Series-series (SS) compensation circuits

This section elaborates the selection and computation of the SS compensation circuits, used in [*S1*].

By using the T-model of the coupling coils, an equivalent circuit of the impedance network is shown by Figure S1.

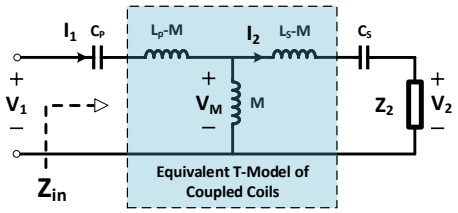

Fig. S1. The impedance network with a T-model of the coupling coils.

By ignoring the internal resistance of the coupling coils, the impedance matrix is given by:

$$\begin{bmatrix} V_1 \\ V_2 \end{bmatrix} = \begin{bmatrix} Z_{11} & Z_{12} \\ Z_{21} & Z_{22} \end{bmatrix} \begin{bmatrix} I_1 \\ I_2 \end{bmatrix} \tag{S1}$$

where,

$$Z_{11} = \frac{V_1}{I_1}|_{I_2=0} = j\omega L_P - \frac{j}{\omega C_P}$$
$$Z_{22} = \frac{V_2}{I_2}|_{I_1=0} = j\omega L_S - \frac{j}{\omega C_S}$$
$$Z_{12} = \frac{V_1}{I_2}|_{I_1=0} = -j\omega M,\ Z_{21} = \frac{V_2}{I_1}|_{I_2=0} = -j\omega M.$$

I_2 is calculated in terms of I_1 as follows:

$$I_2 = -\frac{Z_{21}}{Z_2 + Z_{22}} I_1 \tag{S2}$$

R. Naghash is with the Faculty of Electrical Engineering, Shahid Beheshti University, Velenjak, Tehran, Iran. E-mail: re.naghash@gmail.com

S. M. M. Alavi is with the Department of Electrical and Computer Engineering, University of Windsor, Windsor, ON, Canada. E-mail: mahdi.alavi.work@gmail.com, mahdi.alavi@uwindsor.ca (*Corresponding Author)*

S. E. Afjei is with the Faculty of Electrical Engineering, Shahid Beheshti University, Velenjak, Tehran, Iran. E-mail: e-afjei@sbu.ac.ir

where, Z_2 is the output impedance seen from the input of the rectifier. Thus, V_1 is given by:

$$V_1 = \Big(Z_{11} - \frac{Z_{12}^2}{Z_2 + Z_{22}}\Big) I_1 \tag{S3}$$

The substitution of Z_{12} in (S3) results in:

$$V_1 = \Big(Z_{11} + Z_r\Big) I_1 \tag{S4}$$

where,

$$Z_r = \frac{\omega^2 M^2}{Z_2 + Z_{22}} \tag{S5}$$

is the reflected impedance from the secondary to primary side. As shown in Figure S1, the term $Z_{11} + Z_r$ denotes the input impedance, Z_{in},

$$Z_{in} = Z_{11} + Z_r. \tag{S6}$$

The transmitted power to the secondary side is given by:

$$P = \frac{1}{2}\text{Re}\{Z_{in}\}|I_1|^2 \tag{S7}$$

where, $\text{Re}\{Z_{in}\}$ denotes the real part of Z_{in}. It is deduced from (S4) and (S7) that one way to maximize the power transfer is to make Z_{22} equal to zero, i.e., the secondary side operates at the secondary resonant frequency $\omega_{r,s}$. From (S1) and $Z_{22} = 0$, the relationship between the secondary resonant frequency $\omega_{r,s}$ and C_S and L_S is obtained as follows:

$$\omega_{r,s} = \frac{1}{\sqrt{C_S L_S}}. \tag{S8}$$

By having the secondary resonant frequency $\omega_{r,s}$ and L_S, the secondary compensation capacitor is computed by using (S8).

In addition, unity power factor is of other desired specifications in order to minimize the VA rating of the power supply. This is accomplished when the system operates at zero-phase angle (ZPA) frequency and Z_{in} is purely resistive, i.e., the primary side operates at the primary resonant frequency $\omega_{r,p}$. For the resistive loads, the relationship between the secondary resonant frequency $\omega_{r,p}$ and C_P and L_P is obtained by using (S6) and $\text{Im}\{Z_{in}\} = 0$ as follows:

$$\omega_{r,p} = \frac{1}{\sqrt{C_P L_P}}. \tag{S9}$$

The WPT system is designed such that $\omega_r = \omega_{r,p} = \omega_{r,s}$, thus:

$$\omega_r = \frac{1}{\sqrt{C_P L_P}} = \frac{1}{\sqrt{C_S L_S}} \tag{S10}$$

For the the resistive load R_L, and by ignoring the internal resistance of the coupling coils and rectifier's diodes, Z_{in} at $\omega_r = \omega_{r,p} = \omega_{r,s}$ is given by

$$Z_{in}(\omega_r) = \frac{\omega_r^2 M^2}{R_L}. \tag{S11}$$

It is seen that $\text{Im}\{Z_{in}(\omega_r)\} = 0$, implies that the phase responses at ω_r intersect the ZPA line under the variations on the load and mutual inductance. This concludes the justification that the load and mutual inductance variations do not affect the SS capacitors' values at the secondary resonance frequency. In other compensations circuits, the load and/or mutual inductance variations influence the compensation capacitors, [*S5*]. In SP compensations circuits, the secondary resonance frequency is independent of load, but changes with the mutual inductance. In PP and PS compensations circuits, both the load and mutual inductance variations change the secondary resonance frequency.

Figure S2 shows the frequency response of Z_{in} in bode diagram. It is seen that for various loads, the resonant and ZPA frequencies do not change by using the capacitor-based SS compensation circuits.

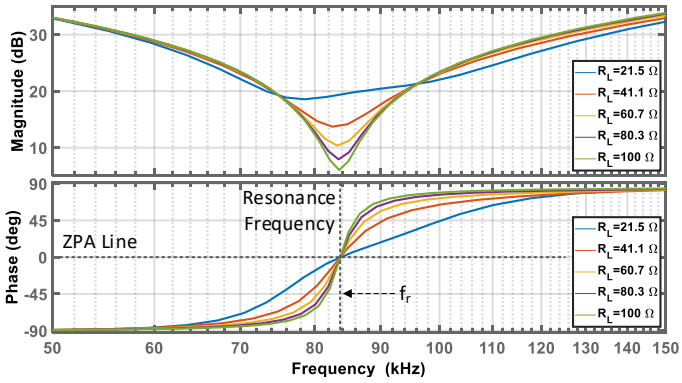

Fig. S2. Bode diagram of the input impedance, Z_{in}, under the load variations for the SS-WPT in [*S1*].

S.II. Model Validation

To verify the accuracy of the driven small-signal transfer function, the circuit is implemented in Matlab Simulink with component values given in Section II of [*S1*]. The response of the circuit to 1% variation of the duty cycle is compared to 1% step response of the transfer function (3) in [*S1*]. The result is shown in Figure S3, which confirms a satisfactory level of accuracy.

S.III. Additional Results

A. QFT-based Robust Control

Figure S4 shows the simulation results of the time-domain step response of the open-loop (uncontrolled) and controlled SS-WPT system, when the load changes from $R_L = 22$ to 100Ω under the perfect wireless communications, i.e., $k = 0$ in (18) in [*S1*]. It is seen that the open-loop system response is outside the desired region, while the QFT-based control shifts all responses between D_l and D_u.

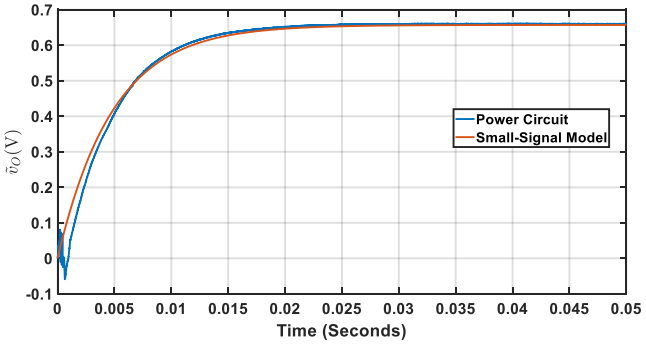

Fig. S3. Comparison between the responses of the circuit and transfer function model (3) in [*S1*].

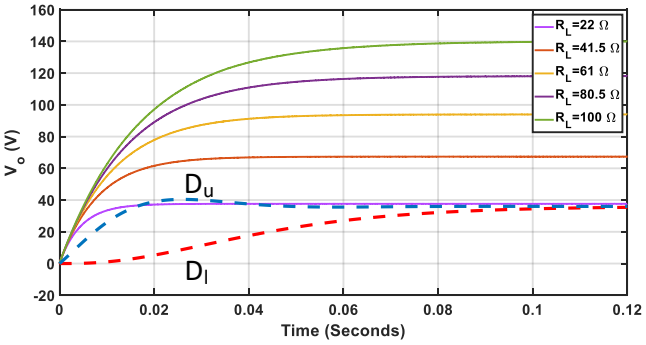

(a) Uncontrolled system.

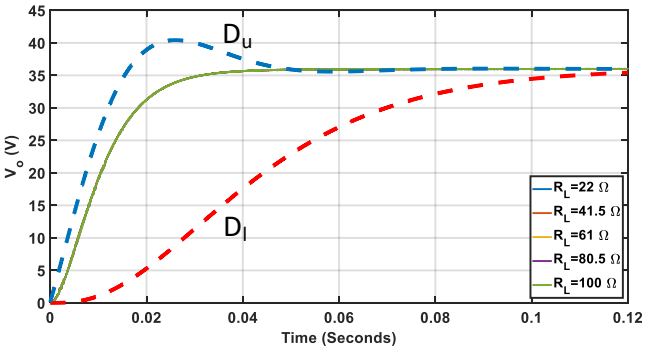

(b) Controlled system

Fig. S4. Simulations: Step response of the SS-WPT system, when load changes from $R_L = 21$ to $100\ \Omega$.

Figure S5 shows the gates' signals S_1 to S_4. It shows that the PWM's duty cycle appropriately changes with respect to the load variations, in order to satisfy the QFT robust control requirements. The signals of the inverters, coils, and rectifies are shown in Figure S6, which match the theoretical principles.

B. Condition to Have Zero-Voltage-Switching (ZVS)

Figure S7 shows the MOSFET's current, drain-source and gate-source voltages of the WPT system controlled by the proposed QFT robust control technique, operating around 50% of duty cycle. It is seen that soft switching is achieved because of the near zero-voltage-switching (ZVS) during the turn on process, and zero-current switching (ZCS) during the turn off. Thus, switching losses are significantly lower than that in

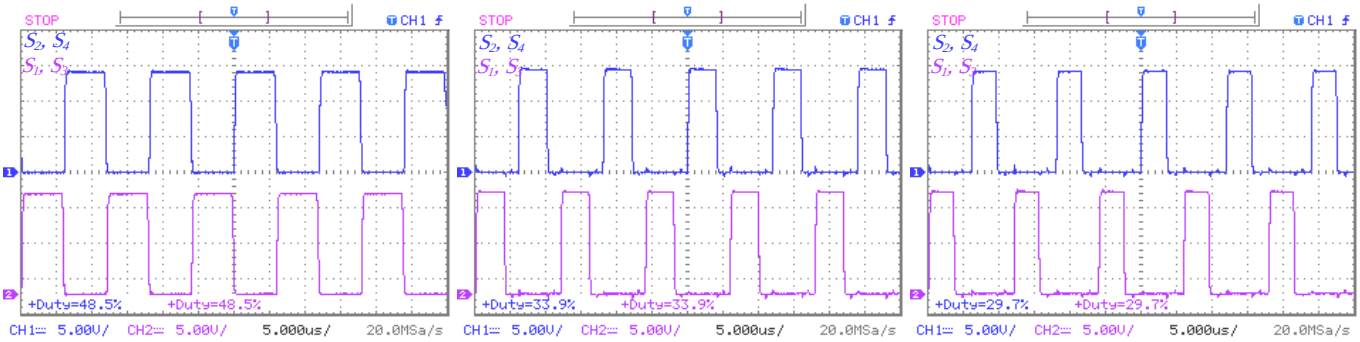

(a) $R_L = 22\Omega$, duty cycle $d = 48.5\%$ (b) $R_L = 32\Omega$, duty cycle $d = 33.9\%$ (c) $R_L = 42\Omega$, duty cycle $d = 29.7\%$

Fig. S5. Experiments: gate signals for various load resistances.

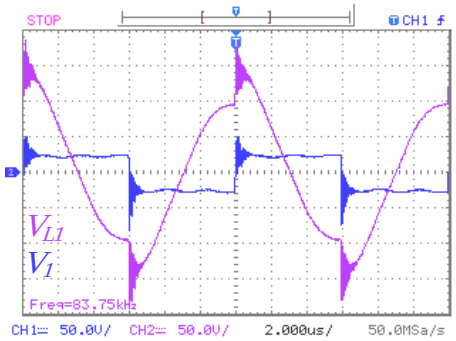

(a) Output voltage of the inverter, and voltage across the primary coil.

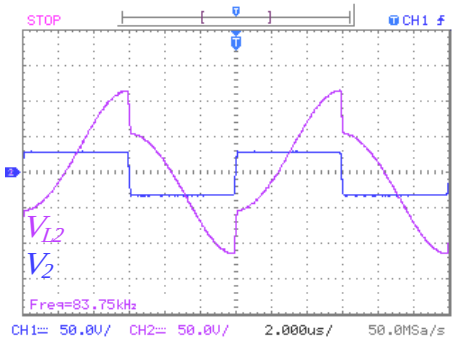

(b) Voltage across the secondary coil, and input voltage of the rectifier.

Fig. S6. Experiments: Voltages of inverter, rectifier, and coils for $R_L = 22\Omega$.

inverters, which are controlled by hard-switching techniques, [*S6*].

During the operation at the resonant frequency, ZVS might be lost if the duty cycle changes. If the appearance of ZVS is also of desired objectives, the input capacitor should be chosen larger. Consider the input capacitor to be increased from $45.1nF$, the value used in [*S1*], to $64nF$. Simulation results show that the designed QFT, H_∞, and SIMC controllers require re-tuning for this much change on the input capacitor, to meet the desired specifications at resonant frequency while having the ZVS at the same time. This is absolutely doable with no new point of principles. Figure S8 shows the simulation result with the new input capacitor, operating at

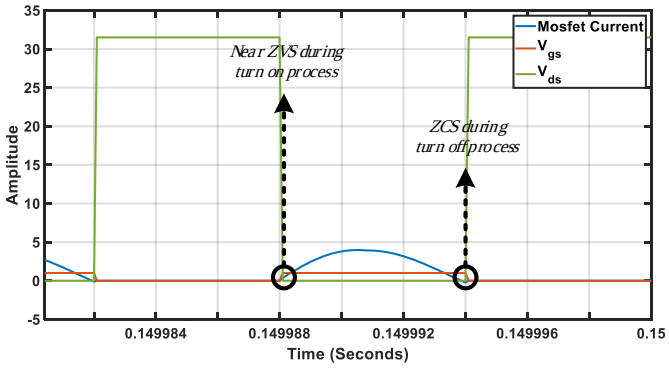

Fig. S7. Illustration of ZVS; with QFT control, duty cycle around 50%, with the input capacitor $45.1nF$.

the duty cycle 40%. It confirms the appearance of ZVS, as the MOSFET turns on after the zero voltage across the drain-source. However, it should be re-mentioned that the transferred power decreases from $58W$ to $32W$ for the load $R_L = 22\Omega$, by increasing the input capacitor.

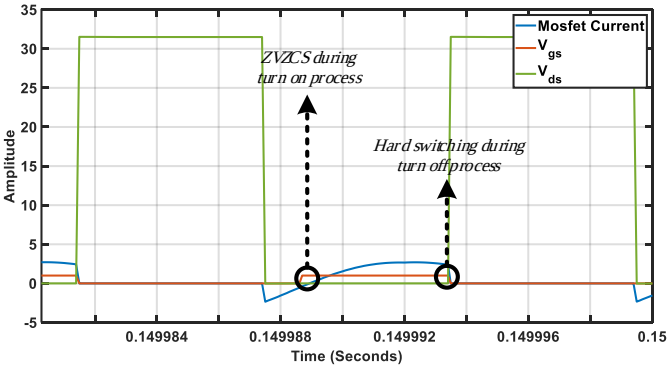

Fig. S8. Illustration of ZVS, with new input capacitor $64nF$. ZVZCS stands for zero-voltage zero-current switching.

S.IV. Comparative Studies

A. The SIMC-based PI Controller

Consider a plant given by:

$$P(s) = \frac{Ke^{-\tau_d s}}{\tau_1 s + 1}. \tag{S12}$$

The SIMC-PI controller

$$G_C = K_C\Big(1+\frac{1}{\tau_I s}\Big) \tag{S13}$$

with

$$K_C = \frac{1}{K}\frac{\tau_1}{\tau_C+\tau_d} \tag{S14}$$

$$\tau_I = \min\{\tau_1, 4\times(\tau_C+\tau_d)\} \tag{S15}$$

guarantees robust tracking and stability performance around the following desired closed-loop system [*S3*, *S4*]

$$T(s) = \frac{1e^{-\tau_d s}}{\tau_C s+1}. \tag{S16}$$

For comparison with the results in [*S1*], a desired $T(s)$ with $\tau_C = 0.029$ and $\tau_d = 3.55\times10^{-6}s$ is chosen, in which its step response is located almost in the middle of D_l and D_u. The chosen τ_d is 5 times the sampling period, which means the SIMC PI controller is designed for the worst case, with the maximum data time-delay. A model $P(s)$ with $K = 2.74$, $\tau_1 = 0.00022$ is arbitrary chosen from the uncertainty region of the open-loop models $\{G_{sys}\}$. Based on these data, and by using (S14) and (S15), the following SMIC-PI control is obtained:

$$G_{C,\text{SIMC}}(s) = 0.0027\Big(1+\frac{1}{2.2\times10^{-4}s}\Big). \tag{S17}$$

Note that in the SIMC-based PI control, no pre-filter is used, i.e., $F(s) = 1$.

B. The H_∞-based PI Controller

The H_∞ PI controller is obtained by using the method in [*S2*], which solves

$$\left\| \begin{array}{c} \gamma^{-1}T \\ D_u^{-1}T \\ W_S S \end{array} \right\|_\infty < 1 \tag{S18}$$

where, the first and second conditions are chosen from the QFT stability and tracking constraints. The third condition is given on the sensitivity function, which should be added to achieve a feasible PI controller. Without the third row condition, a PI controller with very small gain is achieved, which is not desired. The weighting function W_S is chosen as:

$$W_S = \frac{0.8333s+10^4}{s+100}, \tag{S19}$$

which, is complementary to the inverse of D_u^{-1} as shown in Figure S9.

The H_∞ problem is computationally solved by using Matlab's hinfstruct command, and the following PI control is obtained:

$$G_{C,H_\infty}(s) = 0.0632\Big(1+\frac{1}{0.002s}\Big). \tag{S20}$$

Note that in the designed H_∞-based PI control, no pre-filter is used, i.e., $F(s) = 1$.

It should be noted that these robust control techniques could be developed further to address more issues such as over-design and wind-up problems. Interested readers are directed to [*S7*] and [*S8*] for a more comprehensive information.

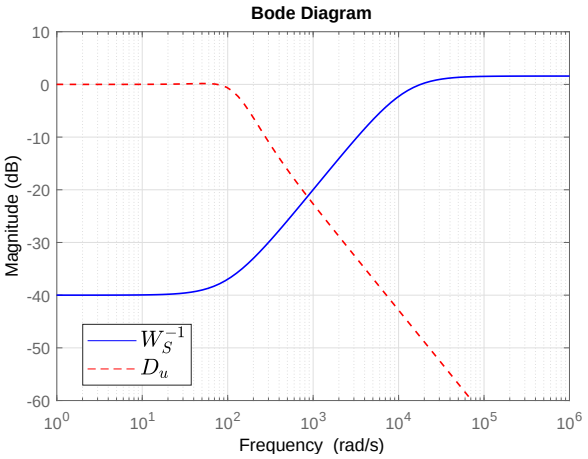

Fig. S9. The H_∞ weighting functions.

REFERENCES

[S1] R. Naghash, S. M. M. Alavi, S. E. Afjei, "Robust Control of Wireless Power Transfer Despite Load and Data Communications Uncertainties," *IEEE Journal of Emerging and Selected Topics in Power Electronics*, DOI: 10.1109/JESTPE.2020.3033001, 2020.

[S2] P. Apkarian and D. Noll, "Nonsmooth H-infinity Synthesis," *IEEE Trans. on Automatic Control*, Vol. 51, No. 1, pp. 71 – 86, 2006.

[S3] S. Skogestad, "Simple analytic rules for model reduction and PID controller tuning," *Journal of Process Control*, Vol. 13, No. 4, pp. 291 – 309, June 2003.

[S4] C. Grimholt, S. Skogestad, "Optimal PI-Control and Verification of the SIMC Tuning Rule," *IFAC Proceedings Volumes*, Vol. 45, No. 3, pp. 11 – 22, 2012.

[S5] Z. Zhang, H. Pang, A. Georgiadis, C. Cecati, "Wireless Power Transfer—An Overview," *IEEE Transactions on Industrial Electronics*, vol. 66, no. 2, pp. 1044 –1058, Feb. 2019.

[S6] H. Matsumoto, Y.Neba, H. Asahara, "Switched Compensator for Contactless Power Transfer Systems," *IEEE Transcations on Power Electronics*, 30 (11), pp. 6120 – 6129, 2015.

[S7] M. J. Walsh, S. M. M. Alavi, M. J. Hayes, "Practical assessment of hardware limitations on power aware wireless sensor networks- an anti-wind up approach," *International Journal of Robust and Nonlinear Control*, Vol. 20, No. 2, pp. 194 – 208, 2010.

[S8] B. Labibi, S. M. M. Alavi, "Inversion-free decentralised quantitative feedback design of large-scale systems," *International Journal of Systems Science*, 47(8), 1772-1782, 2016.